International Journal of Bifurcation and Chaos, Vol. 15, No. 5 (2005) 1615–1624

THE PATH TOWARDS A LONGER LIFE: ON INVARIANT SETS AND THE ESCAPE TIME LANDSCAPE

ERIK M. BOLLT
Department of Mathematics and Computer Science, Clarkson University, Potsdam, NY 13699-5815, USA

Received April 26, 2004; Revised June 22, 2004

Unstable invariant sets are important to understand mechanisms behind many dynamically important phenomenon such as chaotic transients which can be physically relevant in experiments. However, unstable invariant sets are nontrivial to find computationally. Previous techniques such as the PIM triple method [Nusse & Yorke, 1989] and simplex method variant [Moresco & Dawson, 1999], and even the step-and-stagger method [Sweet *et al.*, 2001] have computationally inherent dimension limitations. In the current study, we explicitly investigate the landscape of an invariant set, which leads us to a simple gradient search algorithm to construct points close to the invariant set. While the calculation of the necessary derivatives can be computationally very expensive, the methods of our algorithm are not as dimension dependant as the previous techniques, as we show by examples such as the two-dimensional instability example from [Sweet *et al.*, 2001] followed by a four-dimensional instability example, and then a nine-dimensional flow from the Yoshida equations, with a two-dimensional instability.

Keywords: Chaos; chaotic transient; unstable chaotic saddle; turbulence; PIM; invariant set.

1. Introduction

It has been illustrated that unstable invariant chaotic saddles can strongly influence physical experiments [Sweet *et al.*, 2001] and that chaotic transients can be caused by the presence of nonattracting invariant sets (saddles) [Nusse & Yorke, 1989; Tél, 1990]. For example, long-lived transients in a pipe flow [Darbyshire & Mullin, 1995] imitate turbulent states, making it extremely difficult to determine the precise transition to sustained turbulence if it exists. Unstable chaotic saddles have also been shown to be useful in communication with chaos, since embedded chaotic saddles often exist with substantial channel capacity but important noise resistance properties [Bollt *et al.*, 1997].

Despite their dynamical importance, the fact is that unstable invariant sets have been difficult to construct explicitly. In this article, we present an entirely new and deterministic technique to construct unstable invariant sets, which for the first time has no fundamental obstacles preventing its applications to even higher dimensional dynamical systems. For each point in the space, one can numerically compute a "lifetime", that is how long the trajectory remains in some bounded region. A point that lies on an invariant set in the region will have an infinite lifetime. In practice, the goal is to find points with very long lifetime. The most direct previous method, called the "Sprinkle method" [Kantz & Grassberger, 1985] relies on a uniformly distributed random sampling of initial conditions over the phase space, wherein the chance of finding points closer to the invariant set shrinks exponentially with lifetime, and likewise there are serious difficulties in all but two-dimensional systems due to the simple explosion of space in higher dimensions. The unstable set is

not adequately approximated for computations of ergodic statistics such as Lyapunov exponents on the invariant set. The "PIM-triple" method [Nusse & Yorke, 1989] is a straightforward and now popular technique which works well even in higher overall dimensional systems when the unstable dimension is one. PIM calculates the invariant sets adequately to compute Lyapunov exponents and has been used for example in communicating with chaos [Bollt *et al.*, 1997], in a class-B laser [Schwartz & Carr, 1999] and appropriately modified for experimental NMR laser data [Jánosi & Tél, 1994]. A "PIM-simplex" method has recently been developed by Moresco and Dawson [1999] which is an important generalization, and it can often construct unstable invariant sets in two or more unstable dimensions. However, the technique is complicated and does not work well for some systems. In [Sweet *et al.*, 2001], a particularly simple technique called "step-and-stagger" was developed which works well for one- and two-dimensional unstable dimensional invariant sets, and some more unstable systems. However, step-and-stagger also has a random searching aspect: perturbation directions are chosen random uniformly on an n-sphere and much of its success is due to cleverly choosing the size of the step from an exponential random distribution. Step-and-stagger is surprisingly robust and efficient given its simplicity to implement, for systems which are not too high dimensional. The technique suffers from its random nature in higher dimensions due to the simple explosion of space in higher-dimensions, the so-called curse of dimensionality. The random step (called a "stagger") ignores the local structure of the dynamics.

It is in this historical landscape that we feel that there is a need for a systematic and all-new approach to the problem of finding unstable invariant sets, with no fundamental dimension barriers. We describe the lifetime function landscape, and we describe the directions of improving lifetime, which gives rise to a direct technique to improve lifetime within a desired set corresponding to solving an ordinary differential equation, which essentially follows unstable foliations towards stable manifolds of points on the unstable invariant set. See our own critique of our gradient based method in the conclusion.

Throughout the presentation in the next several sections, we will use the Henon map as an illustrative example, since a map of the plane allows better pictorial illustration than do the high dimensional maps for which the techniques are intended. The Henon map [Hénon, 1976],

$$\mathbf{F}(x, y) = \langle a - x^2 + by, x \rangle, \tag{1}$$

has the famous parameter values, $a = 1.4$, $b = 0.3$.

2. Discrete and Continuous Lifetime Functions

We use notation for a uniformly continuously differentiable discrete-time dynamical system,

$$\mathbf{z}_{n+1} = \mathbf{F}(\mathbf{z}_n), \quad \mathbf{z}_n \in \Re^d, \quad \mathbf{F} \in C^1. \tag{2}$$

We wish to explicitly construct an ϵ-chain, or "pseudo"-orbit segment $\{\mathbf{z}_i\}_{i=0}^N$, that is,

$$\|\mathbf{z}_{n+1} - \mathbf{F}(\mathbf{z}_n)\| < \epsilon, \tag{3}$$

is satisfied [Robinson, 1995]. We require that the orbit lies in some set B. Then we say that $\{\mathbf{z}_i\}_{i=0}^N$ is a *B-invariant orbit segment* if $\mathbf{z}_i \in B$, $\forall\, i = 0, 1, \ldots, N$, and each $\mathbf{z}_i$ satisfies Eq. (2). Exact orbits rarely exist in a finite precision computer and choosing $\epsilon = 10^{-15}$, the order of machine precision, is the best that can be constructed. Define discrete forward (backward) lifetime functions, $L_B^{\pm}\colon \Re^d \to Z^{\pm}$, as follows,

$$L_B^{\pm}(\mathbf{z}) = |j| \quad \text{if } \mathbf{F}^{\pm i}(\mathbf{z}) \in B, \quad \text{for } 0 \le |i| \le |j|, \text{ but } \mathbf{F}^{\pm(j+1)}(\mathbf{z}) \notin B. \tag{4}$$

That is $\mathbf{F}^{\pm i}$ denotes the ith forward or backward iterate, depending on the sign, and $\mathbf{F}^0$ denotes the identity map, $\mathbf{F}^0(\mathbf{z}) \equiv \mathbf{z}$, for all $\mathbf{z}$.

In Fig. 1, we see a lifetime function plotted over the phase space, for the Henon map, Eq. (1), and where B is a circle of radius 2 centered on the origin. We will not explicitly use the following fact, but it is relevant background and a main idea behind a lifetime-improver algorithm even if uniform hyperbolicity is by no means expected to be present in our specific models. Nonetheless we find it instructive to describe the hyperbolic picture. Hyperbolicity shrinks errors upon inverse iteration along unstable manifolds, and along stable manifolds upon forward iterations. To arrive at a point on the stable manifold of some point in an unstable invariant set, it is best to move transversely to that stable manifold, along unstable foliations.

Let,

$$\mathcal{L}_B(i)^{\pm} = \{\mathbf{z}\colon L_B^{\pm}(\mathbf{z}) \ge |i|\}, \tag{5}$$

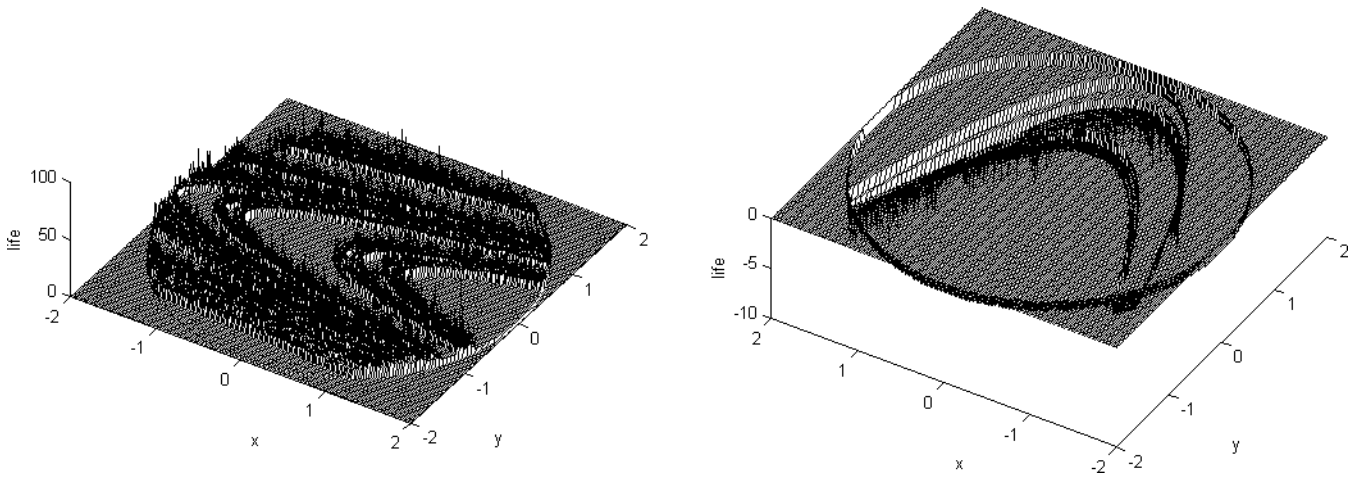

Fig. 1. Forward (left) and backward (right) lifetime functions Eq. (4) of Henon map, Eq. (1), where B is a circle of radius 2 centered on the origin.

be the set of points with lifetime of at least i. This definition helps to explain the towering steps nature of the lifetime functions shown in Figs. 1 and 2; by definition, there is the natural nesting of steps of increasing heights, $\mathcal{L}_B^{\pm}(i \pm 1) \subset \mathcal{L}_B^{\pm}(i)$, $\forall\, i$.

Our job is to construct an algorithm to detect the direction to the next higher step; step-and-stagger makes no such attempt, instead choosing a direction at random. To this end, we introduce the following continuous generalization of the lifetime function. Using the distance function from a point $\mathbf{z}$ to the set B,

$$R_B(\mathbf{z}) = \operatorname{dist}(z, B) = \inf_{\mathbf{y}\in B} \operatorname{dist}(\mathbf{z}, \mathbf{y}), \tag{6}$$

we define the continuous lifetimes, $l_B^{\pm}\colon \Re^d \to \Re$,

$$l_B^{\pm}(\mathbf{z}) = n + \frac{1}{R_B(\mathbf{F}^{\pm n}(\mathbf{z}))}, \quad \text{where } n = L_B^{\pm}(\mathbf{z}). \tag{7}$$

If B is not convex, then the gradient derivative of $l_B^{\pm}(\mathbf{z})$ may not be continuous, which would lead to interesting but unintended consequences. For what follows, we will assume that B is convex.

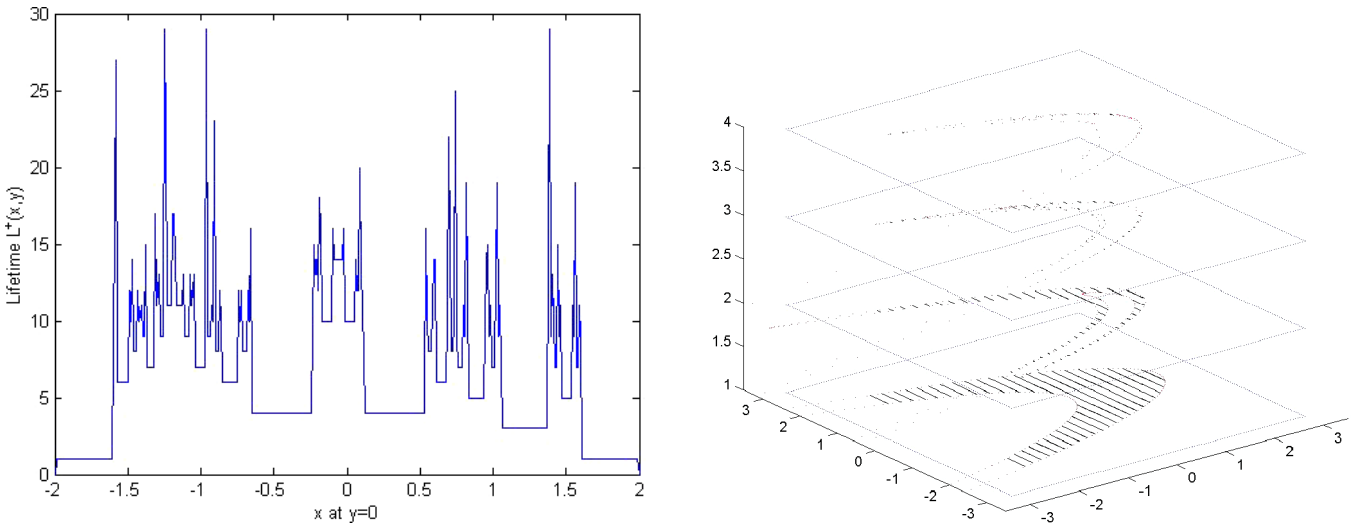

Fig. 2. (Left) A cross-section of the forward lifetime function of Henon map, Eq. (1), shown in Fig. 1, where B is a circle of radius 2 centered on the origin. Notice the stepping nature of the towers of increasing lifetime. (Right) Layers show points invariant in a box $[-2, 2]\times[-2, 2]$ for $i = 1, 2, 3, 4$ steps successively. The spikes limit on the invariant set $\mathcal{L}^{\pm}(\infty)$, approximated in Fig. 4.

The gradient vector for a continuously differentiable function points in the direction of steepest descent, and therefore vectors,

$$\mathbf{u}^{\pm}(\mathbf{z}) = -\nabla l_B(\mathbf{z}), \tag{8}$$

always point locally in the direction of steepest increasing continuous lifetime $l_B^{\pm}(\mathbf{z})$, when $\mathbf{z}$ is in the interior of $\mathcal{L}_B(i)$, a region of fixed and finite discrete lifetime. The Appendix presents a discussion of an alternative geometric way to derive the directions of increasing lifetime function.

Now increasing a lifetime becomes obvious. Increasing lifetime formally corresponds to solving the ordinary differential equation,

$$\frac{d\mathbf{z}}{ds} = -\nabla l_B^{\pm}(\mathbf{z}), \tag{9}$$

where s denotes parameterization along a curve of increasing continuous lifetime invariant in B. We remark that the formulation of the problem of increasing lifetime in terms of ODE Eq. (9) should be considered no more than a formalism, since we do not wish to discuss here questions of existence and uniqueness due to both discontinuity and the severe stiffness which results as solutions $\mathbf{z}(s) \to \mathcal{L}_B(\infty)$. However, we must grapple with the stiffness numerically even when constructing points of lifetimes of say 50 or 60, which we will discuss in the next section.

2.1. *Computing the gradient*

In general, the distance between a point and a set, as described in Eq. (6), is not computationally simple. However, if B is convex, the distance after first escape to the center of B, (denoted by $\mathbf{c}$), is monotone with respect to the set distance $R_B(\mathbf{z})$ in Eq. (6). In fact, monotonicity of the magnitude of the "radial" vectors, with respect to $R_B(\mathbf{z})$ follows for any choice of $\mathbf{c} \in B$. Therefore define the radial vectors,

$$\mathbf{r}^{\pm}(\mathbf{z}) = \mathbf{F}^n(\mathbf{z}) - \mathbf{c}, \quad \text{where } n = L_B^{\pm}(\mathbf{z}), \tag{10}$$

gives the distance to some reference point $\mathbf{c}$ by,

$$d^{\pm}(\mathbf{z}) = \sqrt{\mathbf{r}^{\pm}(\mathbf{z}) \cdot \mathbf{r}^{\pm}(\mathbf{z})} \tag{11}$$

We now redefine the continuous lifetime functions more usefully as,

$$l_B^{\pm}(\mathbf{z}) = n + \frac{1}{d^{\pm}(\mathbf{z})}, \quad \text{where } n = L_B^{\pm}(\mathbf{z}), \tag{12}$$

and $\mathbf{r}^{\pm}(\mathbf{z})$ is calculated as in Eq. (10). However, since

$$\nabla\left(\frac{1}{\sqrt{\mathbf{r}^{\pm}(\mathbf{z}) \cdot \mathbf{r}^{\pm}(\mathbf{z})}}\right) = \left[\frac{-1}{2\sqrt{\mathbf{r}^{\pm}(\mathbf{z}) \cdot \mathbf{r}^{\pm}(\mathbf{z})}}\right]^3 \nabla(\mathbf{r}^{\pm}(\mathbf{z}) \cdot \mathbf{r}^{\pm}(\mathbf{z})), \tag{13}$$

and since the part in the brackets is a scalar factor which does not affect the direction of the gradient vector,[1] we define even more simply,

$$\tilde{l}_B^{\pm}(\mathbf{z}) = n - d^{\pm}(\mathbf{z}), \quad \text{where } n = L_B^{\pm}(\mathbf{z}), \tag{14}$$

which is sufficient to capture the direction of the gradient field for $\mathbf{z}$ for each $\mathcal{L}_B(n)$. The gradients resulting from Eqs. (12) and (14) are parallel, $\nabla l_B^{\pm}(\mathbf{z}) \parallel \nabla \tilde{l}_B^{\pm}(\mathbf{z})$. Here, "$\parallel$" denotes that the two vectors are parallel. Finally, we define the direction vector pointing towards increasing (decreasing) lifetime,

$$\mathbf{v}^{\pm}(\mathbf{z}) = \frac{\nabla l_B^{\pm}(\mathbf{z})}{\sqrt{\nabla l_B^{\pm}(\mathbf{z}) \cdot \nabla l_B^{\pm}(\mathbf{z})}}, \tag{15}$$

which is well defined for $\mathbf{z}$ in the interior of $\mathcal{L}_B(n)$, for each n.

Explictly, the direction of the gradient vector, for $\mathbf{z}$ in the interior of $\mathcal{L}_B(n)$,

$$\nabla l_B^{\pm}(\mathbf{z}) \| \nabla(n - \mathbf{r}^{\pm}(\mathbf{z}) \cdot \mathbf{r}^{\pm}(\mathbf{z})) \| D\mathbf{r}^{\pm}|_{\mathbf{z}} \cdot \mathbf{r}^{\pm}(\mathbf{z}), \tag{16}$$

since $\nabla n = 0$ on each constant life step. The derivative $D\mathbf{r}^{\pm}|_{\mathbf{z}}$ is the composite Jacobian matrix, which by the chain rule,

$$\begin{aligned} D\mathbf{r}^{+}|_{\mathbf{z}} &= D\mathbf{F}^n|_{\mathbf{z}} \\ &= D\mathbf{F}|_{\mathbf{F}^{n-1}(\mathbf{z})} \cdot D\mathbf{F}|_{\mathbf{F}^{n-2}(\mathbf{z})} \cdot \cdots \cdot D\mathbf{F}|_{\mathbf{z}}, \\ D\mathbf{r}^{-}|_{\mathbf{z}} &= D\mathbf{F}^{-n}|_{\mathbf{z}} = D\mathbf{F}^{-1}|_{\mathbf{F}^{-n+1}(\mathbf{z})} \\ &\quad \cdot D\mathbf{F}^{-1}|_{\mathbf{F}^{-n+2}(\mathbf{z})} \cdot \cdots \cdot D\mathbf{F}^{-1}|_{\mathbf{z}}, \end{aligned} \tag{17}$$

and where $D\mathbf{F}$ is the Jacobian of $\mathbf{F}$,

$$D\mathbf{F} = \frac{\partial \mathbf{F}_i}{\partial \mathbf{z}_j}, \quad \text{and} \quad D\mathbf{F}^{-1} = \frac{\partial \mathbf{F}_i^{-1}}{\partial \mathbf{z}_j}. \tag{18}$$

There are striking similarities between Eq. (16) and the theoretical construction of stable and unstable foliations [Jaeger & Kantz, 1997], which we will discuss further in Sec. 6.

[1]The derivatives exist for $\mathbf{z}$ in the interior of $\mathcal{L}_B(n)$, for each n finite, since $\mathbf{F}$ was assumed continuously differentiable, and so is $\mathbf{F}^n$.

3. Numerical Integration Towards Points of Longer Life

For $\mathbf{z}$ in the interior of $\mathcal{L}_B(n)$, the vector $\mathbf{v}^{\pm}(\mathbf{z})$ points towards increasing lifetime. Solving the ODE,

$$\frac{d\mathbf{z}}{ds} = \mathbf{v}^{\pm}(\mathbf{z}), \tag{19}$$

on a given constant life step interior of $\mathcal{L}_B(n)$, brings us near boundary points corresponding to the next higher step.

We use a simple adaptive scheme. Stated as an algorithm,

Algorithm A:

(1) Start at an arbitrary initial point $\mathbf{z}^0$ in the interior of $\mathcal{L}_B(n)$, and choose $k = 0$, and $h = h_{\max}$.
(2) If the point reaches a pre-chosen lifetime goal, $L_B^{\pm}(\mathbf{z}^k) >$ Goal, then Take a test step,

$$\mathbf{y}^{k+1} = \mathbf{z}^k + h\mathbf{v}^{\pm}(\mathbf{z}^k). \tag{20}$$

(3) If the discrete lifetime of $\mathbf{y}^{k+1}$ is better than that of $\mathbf{z}^k$,

$$L_B^{\pm}(\mathbf{y}^{k+1}) > L_B^{\pm}(\mathbf{z}^k), \tag{21}$$

then assign,

$$\mathbf{y}^{k+1} \to \mathbf{z}^{k+1}, \quad \min(2h, h_{\max}) \to h, \quad k+1 \to k. \tag{22}$$

Go to 2.
(4) If the continuous lifetime of $\mathbf{y}^{k+1}$ is better than that of $\mathbf{z}^k$,

$$l_B^{\pm}(\mathbf{y}^{k+1}) > l_B^{\pm}(\mathbf{z}^k), \tag{23}$$

then assign,

$$\mathbf{y}^{k+1} \to \mathbf{z}^{k+1}, \quad \min(2h, h_{\max}) \to h, \quad k+1 \to k. \tag{24}$$

Go to 2.
(5) If the discrete lifetime of $\mathbf{y}^{k+1}$ is not better than that of $\mathbf{z}^k$,

$$L_B^{\pm}(\mathbf{y}^{k+1}) \le L_B^{\pm}(\mathbf{z}^k), \tag{25}$$

then reduce the step size,

$$\frac{1}{2}h \to h, \tag{26}$$

and try again. Go to 2.

In practice, we evaluate the gradiant in Eqs. (15) and (19) by the second-order difference scheme,

$$[\nabla l_B^{\pm}(\mathbf{z})]_i \sim \frac{[l_B^{\pm}(\mathbf{z} + \delta\mathbf{1}_i) - l_B^{\pm}(\mathbf{z} - \delta\mathbf{1}_i)]}{\mathbf{2}\delta}, \tag{27}$$

where $\mathbf{1}_i$ denotes a unit basis vector of all zeros, except a one in the ith index. For both $\mathbf{z} + \delta\mathbf{1}_i$ and $\mathbf{z} - \delta\mathbf{1}_i$ in one constant step in the interior of $\mathcal{L}_B(n)$ for all i, choosing $\delta \sim O(10^{-7})$ gives an error in the derivative direction of order $O(10^{-14})$, which is close to machine precision. This is simpler than directly using the definition, Eqs. (16) and (17), and computationally sufficient. In the notation adopted above, subscripts denote time, or iteration, of the map, and superscripts denote applications of the above algorithm in search for points with longer lifetime.

4. Building an Invariant Pseudo-Orbit

Given the ability to construct points $\mathbf{z}$ with lifetime of N in the set B, constructing a pseudo-orbit results from the following algorithm,

Algorithm B:

(1) Choose a random starting point $\mathbf{z}_0^0 \in B$, and assign $m = 0$, and $k = 0$.
(2) Using initial position $\mathbf{z}_m^0$, construct a point $\mathbf{z}_m^k \to \mathbf{z}_m$ with lifetime of (at least) N in the set B by algorithm A above.
(3) Iterate $\mathbf{z}_{m+1} = \mathbf{F}(\mathbf{z}_m)$, which by definition automatically has a lifetime, $L(\mathbf{z}_k) \ge N - 1$. Assign $m \to m + 1$.
(4) If $L(\mathbf{z}_k) < N$ improve life; go to 2.
(5) Since $L(\mathbf{z}_k) \ge N$, simply iterate. Go to 3.

That the perturbations $\mathbf{z}_m^0 \to \mathbf{z}_m^k$ become small in step 2 follows at least if there is uniform hyperbolicity as described in Sec. 2.

5. Numerical Examples

Example 1: Henon, Two-Dimensions

First we continue with the Henon map example, Eq. (1). Using Algorithm A, we construct the marked path from starting point (circle) to ending point (star), shown in Fig. 3. The circle has a lifetime $L^+ = 3$, whereas the star at the end of the green path has a lifetime of $L^+ = 76$. It is fast and efficient to produce long invariant orbits such as that shown in Fig. 4.

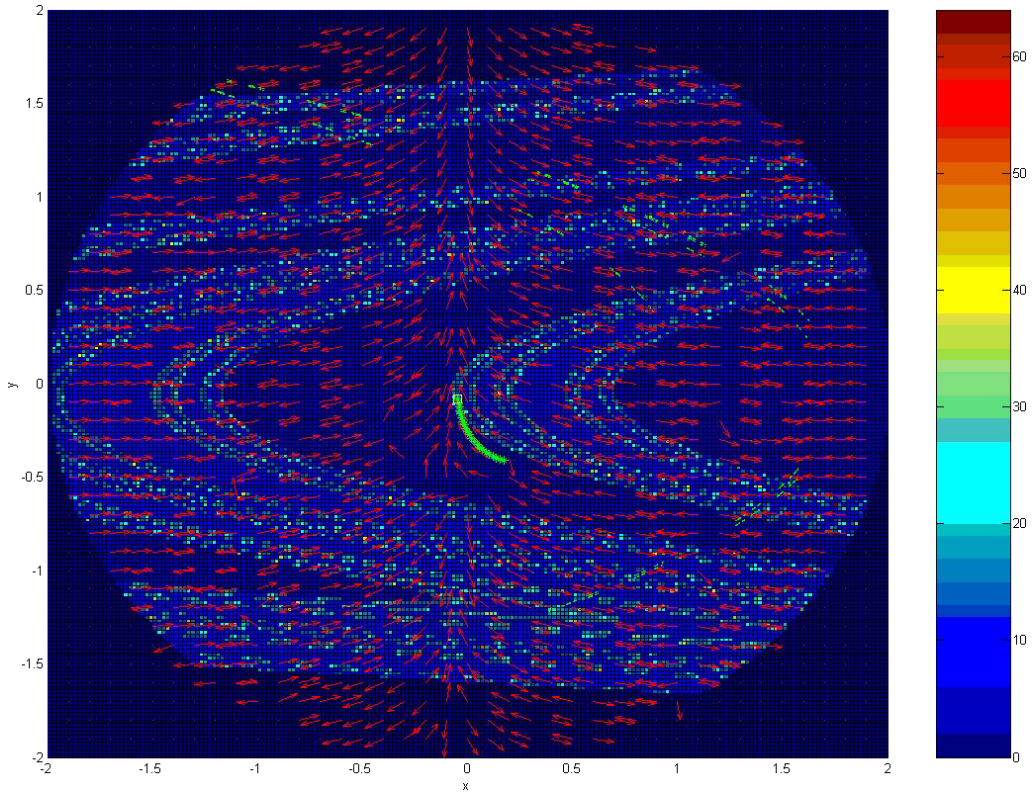

Fig. 3. Algorithm A is used to construct the green path from starting point (circle) with lifetime $L^+ = 3$ to the ending point (star) with lifetime $L^+ = 76$ within B, the circle of radius 2. Direction vector field $\mathbf{v}(\mathbf{z})$ is shown as red arrows, and coloring of each square on grid denotes lifetime L^+ of the square's center point, according to the colorbar scale at right.

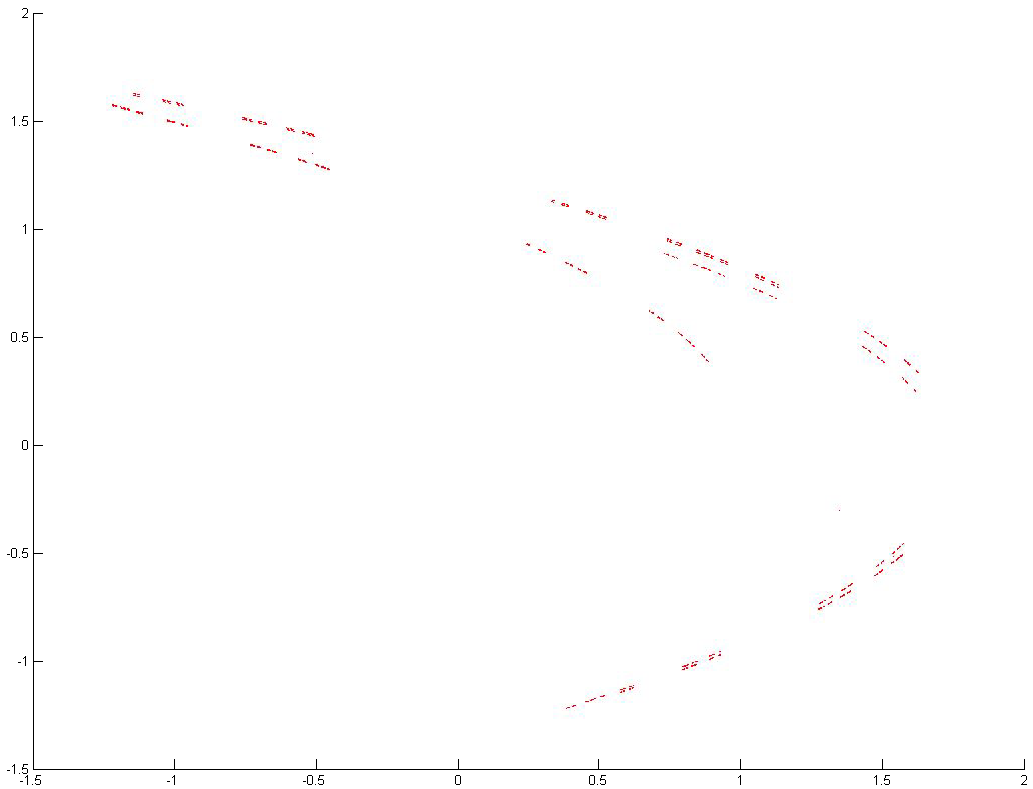

Fig. 4. $\mathcal{L}(60)$ (almost) invariant set of the Henon map, using B as the circle of radius 2.

Example 2: Four-Dimensions, Two-Dimensional Instability

As a second example, in four-dimensions, the algorithm has no problem in reproducing the results of Sweet's paper [Sweet *et al.*, 2001], where using the "step-and-stagger" algorithm, they produced a $\mathcal{L}(30)$ invariant set, for which $\epsilon = 10^{-10}$, for a four-dimensional coupled Henon map,

$$\begin{aligned}\mathbf{F}(x, y, u, v) = (&A - x^2 + By + k(x - u), x,\\ &C - u^2 + Dv + k(u - x), u),\end{aligned} \tag{28}$$

where, $A = 3$, $B = 0.3$, $C = 5$, $D = 0.3$, $k = 0.4$. See Fig. 5. Since the dimension of the instability is 2, due to two positive Lyapunov exponents, the authors in [Sweet *et al.*, 2001] suggested that an instability dimension of ≥ 3 should be the next step, and that their random-direction based search runs slowly when the dimension of possible directions increases.

Example 3: Eight-Dimensions, Four-Dimensional Instability

As an example of higher dimensional instability, we offer the following chain of coupled Henon maps,

$$\begin{aligned}F(\mathbf{x}, \mathbf{y}) = (&a - x_1^2 + by_1, x_1, a - x_2^2 + by_2 + ex_1, x_2,\\ &a - x_3^2 + by_3 + ex_2, x_3,\\ &a - x_4^2 + by_4 + ex_3, x_4),\end{aligned} \tag{29}$$

which when using $(a, b, e) = (1.4, 0.3, 0.001)$, for example, gives the top four Lyapunov exponents $\lambda_+ = (0.0428, 0.0425, 0.0416, 0.0410)$, thus showing a four-dimensional instability embedded in the eight-dimensional phase space. Our algorithm works in this setting, finding for example, the unstable invariant set where $-1.7 \leq x_i \leq 1.7$, $-1.7 \leq y_i \leq 1.7$, $i = 1, 2, 3, 4$.

Example 4: Nine-Dimensional Differential Equation, Two Dimensionally Unstable Poincaré Map

Finally, we give an example motivated by an infinite dimensional embedding space. Starting from a 1D set of PDEs which model nonlinear interactions of magnetic islands in a low-beta tokamak cylindrical plasma, Yoshida *et al.* [1993] derived an $N = 2$ mode interactions model corresponding to 4 ODEs,

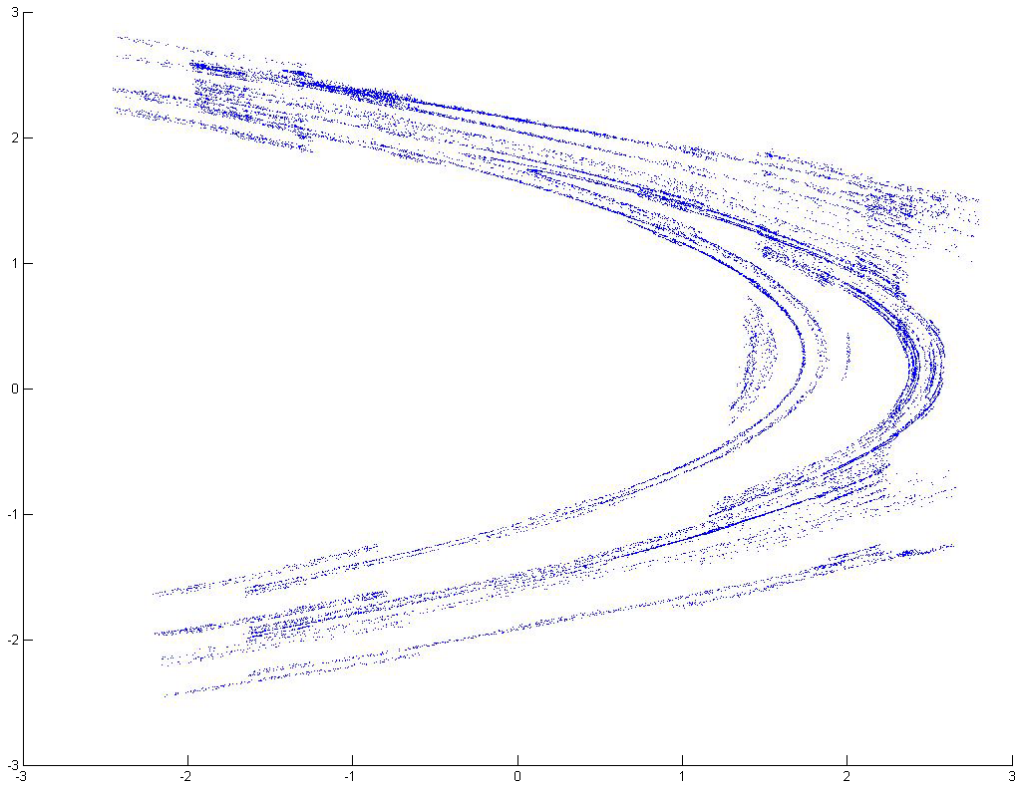

Fig. 5. Invariant set of a four-dimensional coupled Henon map, as in [Sweet *et al.*, 2001].

which was improved to the $N = 3$ modes model giving the following nine-dimensional differential equations [Mirus & Sprott, 1999; Dexter *et al.*, 1991],

$$\begin{aligned}
\dot{y}_1 &= a_1 y_1 y_3^2 + a_2 y_2 y_3,\\
\dot{y}_2 &= a_1 y_2 y_3^2 - a_2 y_1 y_3 + a_3(y_4^2 + y_5^2),\\
&\quad (a_4 - 2y_3 + y_6),\\
\dot{y}_3 &= y_3^2(a_5(y_1^2 + y_2^2)(a_4 - 2y_3 + y_6) + a_6),\\
\dot{y}_4 &= a_1 y_4 y_6^2 + a_2 y_5 y_6,\\
\dot{y}_5 &= a_1 y_5 y_6^2 - a_2 y_4 y_6 + 0.833 a_3(y_7^2 + y_8^2 - y_1^2\\
&\quad - y_2^2)(y_3 - 2y_6 + y_9),\\
\dot{y}_6 &= y_6^2(a_5(y_4^2 + y_5^2)(y_3 - 2y_6 + y_9) + a_6),\\
\dot{y}_7 &= a_1 y_7 y_9^2 + a_2 y_8 y_9,\\
\dot{y}_8 &= a_1 y_8 y_9^2 - a_2 y_7 y_9 + 0.714 a_3(a_7 - y_4^2\\
&\quad - y_5^2)(y_6 - 2y_9),\\
\dot{y}_9 &= y_9^2(a_5(y_7^2 + y_8^2)(y_6 - 2y_9) + a_6),
\end{aligned} \tag{30}$$

where we have chosen $\mathbf{a} = (-0.57813, 1, 9.78195, 0.66811, 5.46545, 0.66126, 3.63998)$. Our interest in this problem is that using the eight-dimensional discrete time mapping resulting from the Poincare' section of negative to positive crossings of the $y_3 = 0$ hyperplane, gives a more substantial higher dimensional problem to test our invariant set finding algorithm. Looking for an invariant set, this time rectangular, hyper-box $B = [-2, 2] \times [-2, 2] \times \cdots \times [-2, 2]$ yields the picture shown in Fig. 6, projected onto the (y_1, y_2) plane. In this case, the top three Lyapunov exponents are, $0.0865, 0.000275, -0.0204$l, indicating a two-dimensional instability. The computational work necessary to find the high-ordered derivatives of a Poincare' map known only through numerically integrating a flow makes for a very long computation, the pixels shown in Fig. 6 taking a good part of a day to compute.

In both Examples 3 (figure not shown) and 4 (Fig. 6), projection from eight to two dimensions

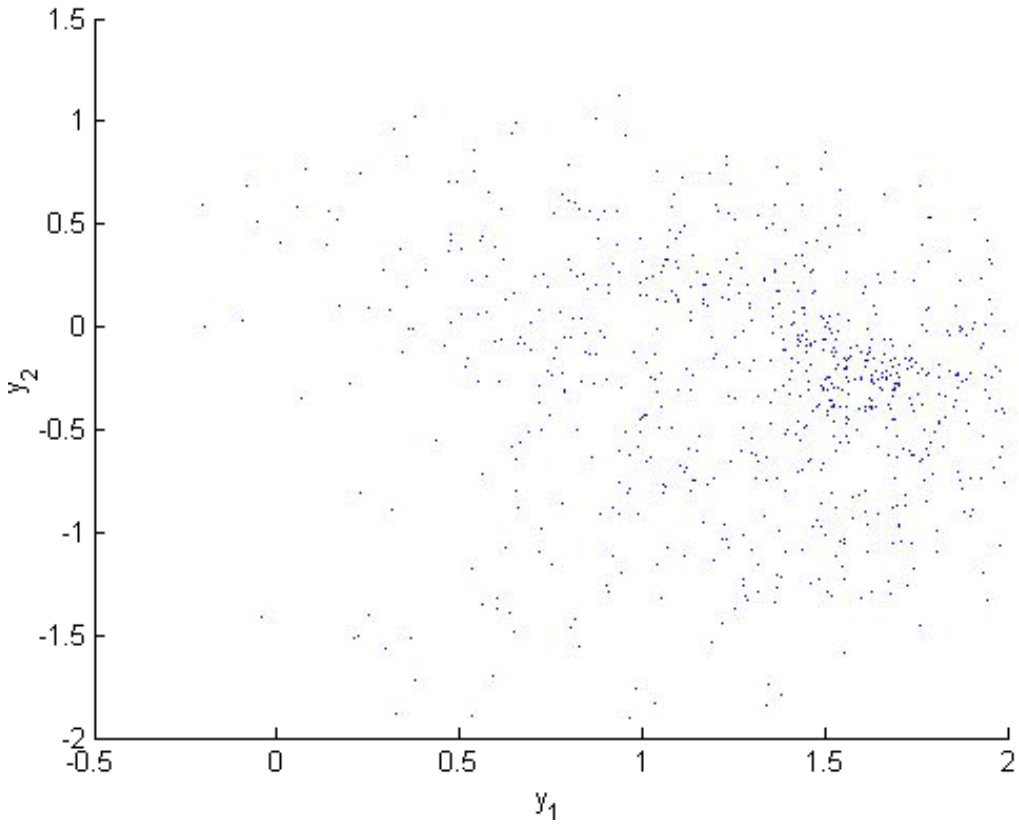

Fig. 6. Invariant set of an eight-dimensional Poincare' mapping of the nine-dimensional Yoshida differential equations Eqs. (30) [Mirus & Sprott, 1999; Dexter *et al.*, 1991]. The projection from eight to two dimensions shown makes it difficult to see the kind of fine structure seen in Figs. 4 and 5.

makes it difficult to display the kind of fine structure seen in Figs. 4 and 5.

6. Stable and Unstable Foliations Versus the Greatest Increasing Lifetime Vector

A stable and unstable foliation of the plane is defined by how the tangent map, the Jacobian matrix of F, rotates an arbitrary vector along orbits, in the tangent space towards the unstable direction, and the Jacobian matrix of the inverse map F^{-1} rotates a vector towards the stable direction [Jaeger & Kantz, 1997]. In practice, we choose an arbitrary unit vector $\mathbf{u}$ and forward multiply, starting at $\mathbf{z}_{-n}$, the Jacobian matrices along the orbit to $\mathbf{z}_0$, normalizing the vector at each step:

$$DF^n|_{z_{-n}} \cdot \mathbf{u} \equiv DF|_{z_{-1}} \cdot DF|_{z_{-2}} \cdot \cdots \cdot DF|_{z_{-n}} \cdot \mathbf{u} \to f_u(\mathbf{z}) \quad \text{as } n \to \infty. \tag{31}$$

Likewise, the stable direction is formed from the inverse Jacobian starting at $T^n(\mathbf{z})$.

$$DF^{-n}|_{z_n} \cdot \mathbf{u} \equiv DF^{-1}|_{z_1} \cdot DF^{-1}|_{z_2} \cdot \cdots \cdot DF^{-1}|_{z_n} \cdot \mathbf{u} \to f_s(\mathbf{z}) \quad \text{as } n \to \infty. \tag{32}$$

This defines the stable and unstable foliations $f_{s,u}(\mathbf{z})$ in the limit, $n \to \infty$. Comparison of Eqs. (31) and (32) to Eqs. (17) reveals a striking similarity when n, the time of first exit in Eqs. (17) is large. The direction vector pointing towards increasing lifetime, $\mathbf{v}^{\pm}(\mathbf{z})$ in Eq. (17), defines a foliation related to the stable and unstable foliations. For large exit time n, $\mathbf{v}^{\pm}(\mathbf{z})$ is almost the same as a stable or unstable vector, at the points $\mathbf{F}^{-n}(\mathbf{z})$ and $\mathbf{F}^{-n}(\mathbf{z})$ respectively. That is, $f_s(\mathbf{F}^{-n}(\mathbf{z}))$ and $f_u(\mathbf{F}^n(\mathbf{z}))$ respectively. So, the vectors we see in Fig. 3, for example, are spatially permuted versions of the unstable foliations, but permuted by $n(\mathbf{z})$ iterates where each n is a function of $\mathbf{z}$. Thus moving from $\mathbf{z}$ in the direction $\mathbf{v}^{\pm}(\mathbf{z})$ generally brings us in a direction which is hoped to be transverse to the stable direction at a future iterate, bringing us almost onto a stable manifold of a point on the invariant set.

7. Conclusions

Here, we have given an all-new approach to the problem of finding unstable invariant sets, with no fundamental dimension barriers. However, our initial hope in beginning this project had been to design a method to cope with high-dimensional differential equations, which display a high-dimensional instability. The inherent calculation of gradients along test orbits requires a great deal of computation for a flow. While effective for lower-dimensional problems, in retrospect, we have found our method expensive to push higher in dimensionality than what is done in our Example 4.

From a descriptive point of view, we have for the first time carefully defined the problems in proper mathematical language with an objective function corresponding to approximating unstable invariant sets, and we have described the lifetime function landscape. We described the directions of improving lifetime, which give rise to a direct technique to improve lifetime within a desired set corresponding to solving an ordinary differential equation, which essentially follows unstable foliations towards stable manifolds of points on the unstable invariant set. We hope that the connections presented in Sec. 6, displayed in Fig. 3, between stable and unstable foliations of the spatially permuted map, and gradients of the lifetime function will inspire interest in their own right.

Acknowledgments

This research was supported by the National Science Foundation under grants DMS-0071314 and 0104087 and by the Keck Foundation.

References

Armstrong, M. A. [1983] *Basic Topology* (Springer Verlag, NY).

Bollt, E. & Meiss, J. D. [1995] "Targeting chaotic orbits to the Moon through recurrence," *Phys. Lett.* **A204**, 373–378.

Bollt, E., Lai, Y. C. & Grebogi, C. [1997] "Analysis of the topological entropy versus noise resistance tradeoff when communicating with chaos," *Phys. Rev. Lett.* **79**, 3787–3790.

Darbyshire, A. G. & Mullin, T. [1995] "Transition to turbulence in constant-mass-flux pipe flow," *J. Fluid Mech.* **289**, 83–114.

Dexter, R. N., Kerst, D. W., Lovell, T. W., Prager, S. C. & Sprott, J. C. [1991] "The Madison symmetric torus," *Fusion Technol.* **19**, 131–139.

Hénon, M. [1976] "A two dimensional mapping with a strange attractor," *Commun. Math. Phys.* **50**, 69–77.

Jaeger, L. & Kantz, H. [1997] "Homoclinic tangencies and non-normal Jacobians — effects of noise in nonhyperbolic systems," *Physica* **D105**, 79–96.

Jánosi, I. M. & Tél, T. [1994] "Time series analysis of transient chaos," *Phys. Rev.* **E49**, p. 2756.

Kantz, H. & Grassberger, P. [1985] "Repellers, semi-attractors and long-lived chaotic transients," *Physica* (Amsterdam) **D17**, 75–85.

Mirus, K. A. & Sprott, J. C. [1999] "Controlling chaos in low- and high-dimensional systems with periodic parametric perturbations," *Phys. Rev.* **E59**, 5313–5324.

Moresco, P. & Dawson, S. P. [1999] "The PIM-simplex method: An extension of the PIM-triple method to saddles with an arbitrary number of expanding directions," *Physica* (Amsterdam) **D126**, 38–48.

Nusse, H. E. & Yorke, J. A. [1989] "A procedure for finding numerical trajectories on chaotic saddles," *Physica* (Amsterdam) **D36**, p. 137.

Robinson, C. [1995] *Dynamical Systems*: *Stability*, *Symbolic Dynamics*, *and Chaos* (CRC Press, Ann Arbor, MI).

Schwartz, I. B. & Carr, T. W. [1999] "Bi-instability as a precursor to global mixed-mode chaos," *Phys. Rev.* **E59**, 6658–6661.

Sweet, D., Nusse, H. E. & Yorke, J. A. [2001] "Yorke 'stagger-and-step' method: Detecting and computing chaotic saddles in higher dimensions," *Phys. Rev. Lett.* **86**, p. 2261.

Tél, T. [1990] in *Direction in Chaos*, ed. Hao, B.-L. (World Scientific, Singapore), p. 149.

Yoshida, Z., Sakuragi, Y. & Yamakoshi, Y. [1993] "A reduced model of chaotic magnetic fluctuations in a tokamak plasma," *J. Plasma Phys.* **49**, p. 403.

Appendix: Inward Pointing Perturbations

A local increase of the continuous lifetime function Eq. (7) by its gradiant is the basis of Algorithm A, but the local increase can also be derived by a geometric demand that perturbations upon first exit must point back towards the exited set. See Fig. 7. Consider contours of equal distance Eq. (6), $\{\mathbf{z} : \mathbf{z} \notin B, R_B(\mathbf{z}) = k, k > 0\}$, which are also locally level surfaces of the continuous lifetime function Eq. (7).

We wish to define the small pertubations upon first exit which point back towards the exited set. See Fig. 7. Starting at a point $\mathbf{z} \in B$, then after first exit from B, at $\mathbf{F}^n(\mathbf{z})$, the vector $\mathbf{q}$ is the inward pointing vector which points directly back to B, which is the normal that defines a half-plane of "bad" perturbations (gray). Any vector $\mathbf{x}$ in the complement, "good" half-plane is defined,

$$(\mathbf{q}, \mathbf{x}) > 0, \tag{A.1}$$

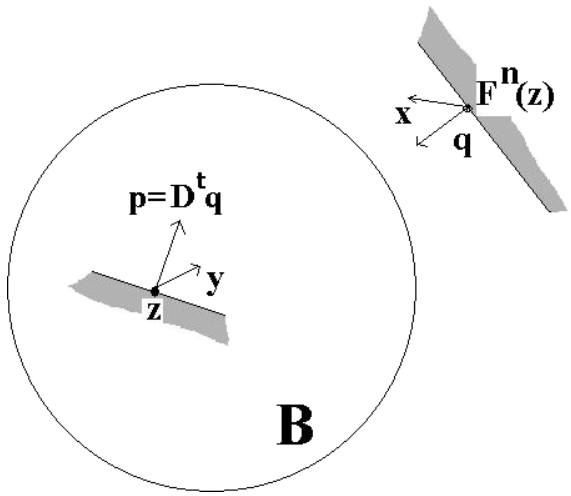

Fig. 7. Pulling back inward point vector $\mathbf{q}$ after first exit from B, to $\mathbf{p}$ in tangent space.

for an inner-product, $(\cdot, \cdot)$. Define the vector $\mathbf{p}$ in the tangent space to be the pulled-back (pre-iterate) of the normal vector $\mathbf{q}$. We wish to calculate $\mathbf{p}$, since it defines the plane of vectors which will be inward pointing after first exit at $\mathbf{F}^n(\mathbf{z})$.

Let,

$$D\mathbf{y} = \mathbf{x}, \tag{A.2}$$

where we have abbreviated,

$$D \equiv D\mathbf{F}^n|_{\mathbf{z}}, \tag{A.3}$$

is the tangent map at $\mathbf{z}$; see Eq. (17). Then substitution of Eq. (A.2) into Eq. (A.4) gives,

$$(\mathbf{q}, D\mathbf{y}) > 0, \tag{A.4}$$

from which follows,

$$(D^t\mathbf{q}, \mathbf{y}) > 0, \tag{A.5}$$

where with respect to the inner product $(\cdot, \cdot)$, D^t denotes the adjoint of D, or transpose since D is a real matrix. Therefore, the vector,

$$\mathbf{p} = D^t\mathbf{q}, \tag{A.6}$$

is the normal of the half-plane of "good" perturbations which will push forward under the tangent map to the half-plane of inward pointing vectors. One could use this vector $\mathbf{p}$ with success in Algorithm A.